Journal of Electronic Research and Application, 2024, Volume 8, Issue 5
http://ojs.bbwpublisher.com/index.php/JERA
ISSN Online: 2208-3510
ISSN Print: 2208-3502

Design and Analysis of Terminal Guidance Law for Kinetic Interceptors based on Pulse Engine

Shixin Li[1], Jia Ma[2], Shuai Yue[1,3,4]*

[1]School of Mechanical Engineering, Nanjing University of Science and Technology, Nanjing 210094, China
[2]Aerospace System Engineering Shanghai, Shanghai 201100, China
[3]Shanghai Key Laboratory of Spacecraft Mechanism, Shanghai 201108, China
[4]National Key Laboratory of Space Intelligent Control, Beijing 100048, China

***Corresponding author:** Shuai Yue, yueshuai@njust.edu.cn

Abstract: A new terminal guidance law is proposed based on a solid propellant pulse engine and an improved proportional navigation method to address the terminal guidance issue for kinetic interceptors. On this basis, the start-stop curve of the pulse motor during the terminal guidance process is designed, along with its start-up logic. The effectiveness of the proposed guidance strategy is verified through simulation.

Keywords: Pulse engine; Terminal guidance law; Kinetic interceptor; Proportional navigation method

Online publication: September 30, 2024

1. Introduction

As a high-speed spacecraft operating outside the atmosphere, kinetic interceptors utilize the enormous kinetic energy generated by high-speed flight to destroy incoming targets through direct collision. Compared to traditional atmospheric-guided weapons, kinetic interceptors employ direct force to control the projectile's attitude, achieving precise interception. Thus, the design of guidance laws is crucial for the precise interception capabilities of kinetic weapons [1]. Current terminal guidance methods mainly address accuracy issues by adding proportional navigation enhancements or adjusting proportional navigation coefficients [2–5]. Previous studies present line-of-sight angular velocity measurements in the design process of terminal guidance laws [6,7]. Research on guidance laws based on proportional navigation mainly focuses on stationary and slow-moving targets [8–10]. For intercepting high-speed targets, the high speed greatly limits the range of line-of-sight angle changes, making it difficult to achieve collision angle constraints for high-speed moving targets. Regarding this problem, previous literature proposed a along/against track guidance law with collision angle constraints, but this solution can only target non-maneuvering targets [11]. On this basis, another study further extended this scheme to high-speed maneuvering targets [12].

In practical applications, the fuel carried by kinetic interceptors is limited, and we hope to complete interception missions with minimum fuel consumption. Fuel consumption is related to the frequency of engine

on/off cycles and the total engine running time, necessitating the selection of an optimal set of engine switching thresholds to minimize energy consumption while successfully hitting the target. Previous researchers have conducted studies on the issue of energy optimization in spacecraft using genetic algorithms or support vector machines [13–15]. For the optimal energy issue of kinetic interceptors, most approaches involve modifying guidance laws to reduce engine switching frequencies, thereby minimizing fuel consumption. Additionally, a study utilized pulse width modulation to reduce engine switching frequency, but simulation results show that the frequency remains high for maneuvering targets [16]. Another study employed a back propagation (BP) neural network algorithm to reduce fuel consumption, but it does not analyze optimization effects for maneuvering targets, and the algorithm implementation is complex [17].

2. Dynamics model

2.1. Interceptor dynamics model

During flight, the dynamics equations for the kinetic interceptor under a ballistic coordinate system can be expressed as:

$$\begin{aligned} &\frac{1}{g}\frac{dv_{\mathrm{m}}}{dt}=\mathrm{n}_x-\sin\theta_m \\ &\frac{v_m}{g}\frac{d\theta_m}{dt}=n_y-\cos\theta_m \\ &-\frac{v_m}{g}\cos\theta\frac{d\psi_v}{dt}=n_z \end{aligned} \tag{1.1}$$

In the equation, v_m, θ_m, and ψ_v represent the interceptor's flight speed, trajectory inclination angle, and trajectory deviation angle. n_x, n_y, and n_z represent the tangential, normal, and binormal overload; g represents gravitational acceleration.

2.2. Relative motion equation

During the guidance process, the relative motion relationship between the interceptor and the target is illustrated in the figure below, where M represents the interceptor and TTT represents the target.

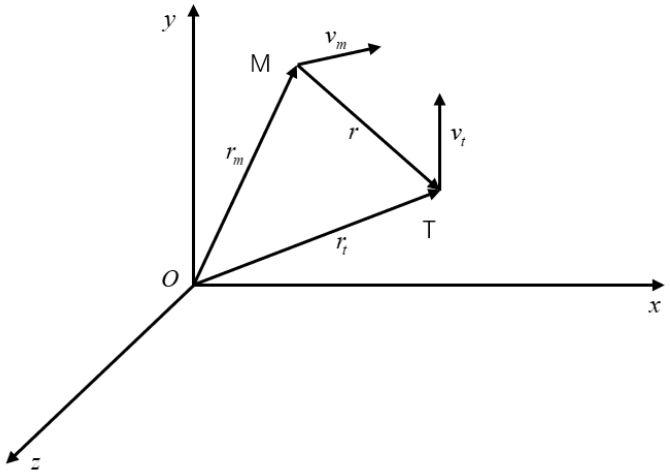

Figure 1. Relative motion relationship between the interceptor and the target

If the interceptor is oriented towards the target along the line of sight, the relative position vector between the interceptor and the target can be expressed as:

$$\boldsymbol{r} = \boldsymbol{r}_t - \boldsymbol{r}_m = r\boldsymbol{e}_r \tag{1.2}$$

Where r_m is the position vector of the kinetic interceptor, r_t is the position vector of the target, e_r is the unit vector in the direction of the line of sight, r is the length of the line of sight.

The line-of-sight rotating coordinate system is defined by the unit vector e_r, in the line-of-sight direction, the unit vector e_ω of the instantaneous angular velocity of the line of sight, and a unit vector e_θ orthogonal to both

$$\begin{aligned} \boldsymbol{e}_r &= \frac{\boldsymbol{r}}{r} \\ \boldsymbol{e}_\theta &= \boldsymbol{e}_\omega \boldsymbol{e}_r \\ \boldsymbol{e}_\omega &= \frac{\boldsymbol{\grave{u}}}{\omega} \end{aligned} \tag{1.3}$$

Where $\grave{u}$ represents the instantaneous angular velocity of the line of sight, ω represents the instantaneous angular velocity rate of the line of sight. According to the vector differentiation rules, it can be obtained that:

$$\dot{e}_r = \omega e_r = \omega e_\omega e_r = \omega e_\theta \tag{1.4}$$

$$\ddot{\boldsymbol{e}}_r = \dot{\omega}\boldsymbol{e}_\theta + \omega\dot{\boldsymbol{e}}_\theta = \dot{\omega}\boldsymbol{e}_\theta - \omega^2\boldsymbol{e}_r \tag{1.5}$$

Differentiating **Equation (1.2)** yields:

$$\dot{\boldsymbol{r}} = \dot{r}\boldsymbol{e}_r + r\dot{\boldsymbol{e}}_r = \dot{r}\boldsymbol{e}_r + r\omega\boldsymbol{e}_\theta \tag{1.6}$$

Differentiating **Equation (1.6)** yields:

$$\ddot{\boldsymbol{r}} = \ddot{r}\boldsymbol{e}_r + 2\dot{r}\dot{\boldsymbol{e}}_r + r\ddot{\boldsymbol{e}}_r \tag{1.7}$$

Combining **Equations (1.4)** and **(1.5)** results in:

$$\ddot{\boldsymbol{r}} = (\ddot{r} - r\omega^2)\boldsymbol{e}_r + (2\dot{r}\omega + r\dot{\omega})\boldsymbol{e}_\theta \tag{1.8}$$

Let a_m and a_t represent the accelerations of the interceptor and the target, respectively. Their expressions in the line-of-sight rotating coordinate system are:

$$\begin{aligned} \boldsymbol{a}_m &= a_{mr}\boldsymbol{e}_r + a_{m\theta}\boldsymbol{e}_\theta + a_{m\omega}\boldsymbol{e}_\omega \\ \boldsymbol{a}_t &= a_{tr}\boldsymbol{e}_r + a_{t\theta}\boldsymbol{e}_\theta + a_{t\omega}\boldsymbol{e}_\omega \end{aligned} \tag{1.9}$$

Where a_{mr} and a_{tr} are the tangential accelerations of the kinetic interceptor and the target, $a_{m\theta}$ and $a_{t\theta}$ are the normal accelerations of the kinetic interceptor and the target, $a_{m\omega}$ and $a_{t\omega}$ are the binormal accelerations of the kinetic interceptor and the target. The relative acceleration between the kinetic interceptor and the target can be expressed as:

$$\ddot{\boldsymbol{r}} = \boldsymbol{a}_t - \boldsymbol{a}_m = (a_{tr} - a_{mr})\boldsymbol{e}_r + (a_{t\theta} - a_{m\theta})\boldsymbol{e}_\theta + (a_{t\omega} - a_{m\omega})\boldsymbol{e}_\omega \tag{1.10}$$

Derive the equations of relative motion:

$$\begin{aligned} \ddot{r} - r\omega^2 &= a_{tr} - a_{mr} \\ 2\dot{r}\omega + r\dot{\omega} &= a_{t\theta} - a_{m\theta} \end{aligned} \tag{1.11}$$

3. Design and implementation of interceptor guidance law

The guidance scheme is based on the idea of suppressing the target's line-of-sight angular velocity using proportional navigation within the atmosphere. It utilizes the difference between the interceptor's heading angle and the target's line-of-sight angle as a control metric, maintaining this difference within a specific range to control the final error.

The interceptor uses a pulse engine for trajectory correction. Since the pulse engine can only be activated in discrete events and cannot be shut off once started, providing a constant impulse, it is necessary to discretize the guidance law, implementing the interceptor's guidance scheme as a sequence of pulses.

The target's position and velocity information required for guidance are measured by the launch platform and transmitted to the interceptor, while the interceptor's position and velocity information are obtained through its onboard inertial navigation system.

$$a_n = K_1 v_m \dot{q} + g_c \cos\theta \tag{1.12}$$

$$a_n = \frac{I_c}{mT_c}$$

$$\Delta V_n = a_n \cdot \Delta t$$

In the equation, a_n is the lateral acceleration required by the interceptor, K_1 is the proportional navigation coefficient, Δt is the control time interval, v_m is the relative flight speed of the projectile to the target, $\dot{q}$ is the rate of change of the line-of-sight angle, g_c is the difference in gravitational acceleration experienced by the projectile and target, θ is the flight speed deviation angle, I_c is the impulse produced by the pulse engine, m is the mass of the interceptor, T_c is the total operating time of the pulse engine.

Over discrete intervals, velocity corrections provided by multiple pulse engines adjust the projectile's relative speed to be parallel to the line connecting the projectile and the target. The principle of the modified proportional navigation method is shown in **Figure 2**.

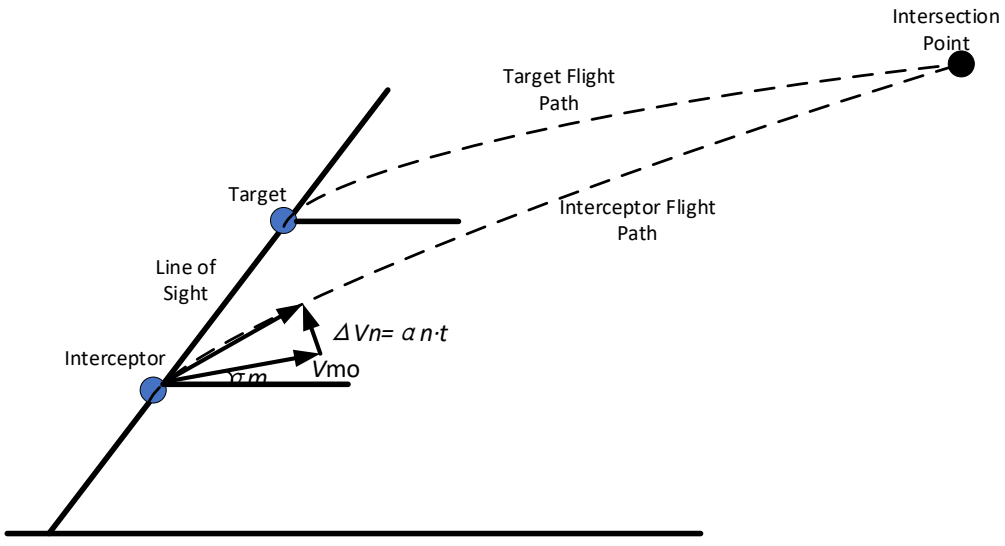

Figure 2. Diagram of the modified proportional navigation guidance principle

At the initial moment of terminal guidance, let the interceptor's position vector be $r_{l0} = (x_{l0}, y_{l0})$ (0,0) initial velocity v_{l0}, initial line-of-sight angle λ initial heading angle psi_0, velocity component along the y-axis $v_{l0y} = v_{l0}$cos

psi_0, and velocity component along the x-axis $v_{l0x} = v_{l0x} \cdot \sin psi_0$.

At the initial moment of terminal guidance, let the target's position vector be $r_{m0} = (x_{m0}, y_{m0})$ (0,10000), velocity component along the y-axis $v_{m0y} = 0$, velocity component along the x-axis $v_{m0x} = 0$, and the magnitude of the target's velocity $v_{mo} = v_{moy}^2 + v_{mox}^2$.

The initial relative position between the interceptor and the target, including the difference in distance along the x-axis and y-axis, is:

$$\Delta y_0 = y_{m0} - y_{l0} \tag{1.13}$$

$$\Delta x_0 = x_{m0} - x_{l0} \tag{1.14}$$

Initial relative position is:

$$\vec{R}_0 = (\Delta y_0, \Delta x_0) \tag{1.15}$$

Initial distance is:

$$\left|\vec{R}_0\right| = \sqrt{\Delta y_0^2 + \Delta x_0^2} \tag{1.16}$$

The position of the target at time t is:

$$\begin{cases} y_{mt} = y_{m0} + v_{m0y} * dt \\ x_{mt} = x_{m0} + v_{mox} * dt \end{cases} \tag{1.17}$$

The position of the interceptor at time t is:

$$\begin{cases} y_{lt} = y_{l0} + v_{l0y} * dt \\ x_{lt} = x_{l0} + v_{lox} * dt \end{cases} \tag{1.18}$$

The relative position between the target and interceptor at time t is:

$$\vec{R}_t = (\Delta y_t, \Delta x_t) \tag{1.19}$$

$$\begin{cases} \Delta y_t = (y_{m0} + v_{m0y} * dt) - (y_{l0} + v_{l0y} * dt) \\ \Delta x_t = (x_{m0} + v_{m0x} * dt) - (x_{l0} + v_{l0x} * dt) \end{cases} \tag{1.20}$$

The distance between the target and interceptor at time t is:

$$\left|\vec{R}_t\right| = \sqrt{\Delta y_t^2 + \Delta x_t^2} \tag{1.21}$$

The relative velocity between the target and interceptor at time t is:

$$\vec{V}_t = (\Delta v_y, \Delta v_x) \tag{1.22}$$

$$\begin{cases} \Delta v_x = v_{mx} - v_{lx} \\ \Delta v_y = v_{my} - v_{ly} \end{cases} \tag{1.23}$$

$$\vec{V}_t = \frac{\vec{R}_t - \vec{R}_0}{dt} \tag{1.24}$$

The component of relative velocity along the normal to the line connecting the projectile and target is:

$$\vec{V}_{tac} = \frac{(\vec{R}_1 \cdot V_2 - \vec{R}_2 \cdot V_1)}{|R_0|} \tag{1.25}$$

$$v_{ta} = \left|\vec{V}_{tac}\right| \tag{1.26}$$

The velocity of the interceptor is:

$$\left|\boldsymbol{v}_I\right| = \sqrt{v_{lx}{}^2 + v_{ly}{}^2} \tag{1.27}$$

The velocity direction angle of the interceptor is:

$$ang_{vl} = \arctan(v_{ly}, v_{lx}) \tag{1.28}$$

The line-of-sight angle of the interceptor is the azimuthal angle of the target relative to the interceptor in the coordinate system, namely:

$$\lambda = \arctan(\dot{\boldsymbol{R}}_2, \dot{\boldsymbol{R}}_1) \tag{1.29}$$

The time derivative of the line-of-sight angle is the rate of change of the line-of-sight angle :

$$\frac{d\lambda}{dt} = \frac{(\dot{\boldsymbol{R}}_1 \mathbf{g} \dot{\boldsymbol{V}}_2 - \dot{\boldsymbol{R}}_2 \mathbf{g} \dot{\boldsymbol{V}}_1)}{\left|\boldsymbol{R}\right|^2} \tag{1.30}$$

4. Pulse engine startup curve design

4.1. Determination of maneuver moments

In the mission, the accuracy is closely related to the angle between the interceptor's velocity direction and the target's line of sight. However, each pulse engine of a space interceptor can only be used once. Therefore, when to activate the engine for correction must be designed based on mission requirements. To make the terminal guidance law of the interceptor more feasible in engineering, it is first necessary to determine the error limits for final accuracy based on the mission's navigation precision requirements. The maximum lateral correction impulse that a single pulse engine can provide is a fixed value within a small error range. Hence, a startup threshold must be set for the computer on the interceptor to determine when to execute the guidance algorithm. Then, based on the calculation results, determine the required impulse, thus determining how many engines need to be started to achieve the velocity increment required by the guidance law. After starting the track control engines one by one, no further control is applied.

This guidance rate takes the angle between the interceptor's velocity direction and the target's line of sight as the engine's startup threshold. If the threshold is set too high, it can cause the target to be outside the interceptor's seeker detection range, losing the target. If the threshold is set too low, it can lead to frequent startup of the pulse engines, increasing the load on the interceptor's computer. Moreover, frequent corrections can cause the velocity direction to oscillate back and forth on both sides of the target line, although it increases tracking accuracy, it requires more engines and computer hardware resources, thus increasing mission costs.

Set the engine startup threshold to $\beta = \lambda$- *psi* = ±9° based on the conical detection range of the seeker head. The threshold can be reduced according to mission accuracy requirements and the number of pulse engines. Combining the above guidance principles and calculation methods, the algorithm workflow of the computer on the interceptor is shown in **Figure 3**.

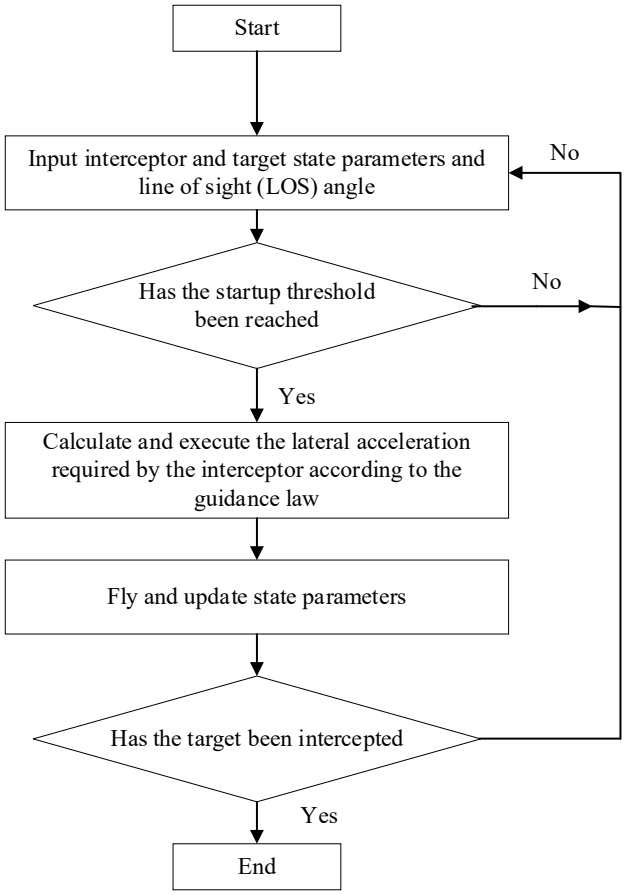

Figure 3. Terminal guidance decision process flowchart

5. Startup logic design

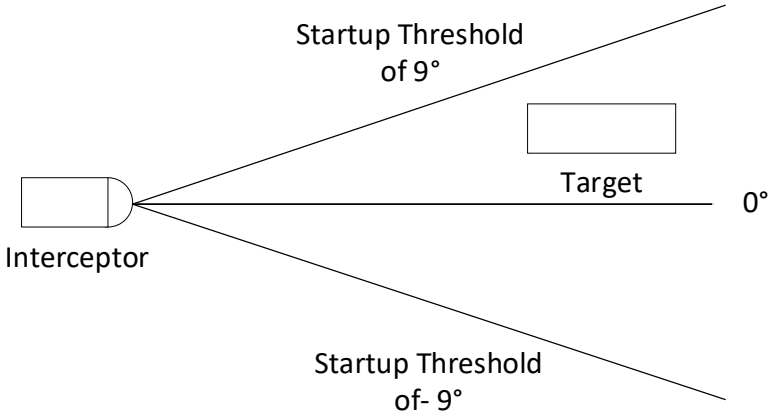

Figure 4. Startup threshold diagram

The logic design for the pulse engine startup determination is as follows:

(1) If the seeker head detects $\beta = \lambda - psi \geq \pm 9°$, then increase the computed value of Δv_n to be positive.

(2) If the seeker head detects $\beta = \lambda - psi \leq -9°$, then decrease the computed value of Δv_n to be negative.

(3) If the seeker head detects $0° - \beta = \lambda - psi \leq 9°$, further calculate the component of the interceptor's relative speed to the target along the normal to the line connecting the projectile and target. If $v_x \geq 3$m/s, then round up the calculated value of Δv_n.

(4) If the seeker head detects $0° \leq \beta = \lambda - psi \leq 9°$, further calculate the component of the interceptor's relative speed to the target along the normal to the line connecting the projectile and target. If $v_x \leq$ -3m/s, then round down the calculated value of Δv_n.

(5) If the seeker head detects $0° \leq \beta = \lambda - psi \leq 9°$, further calculate the component of the interceptor's relative speed to the target along the normal to the line connecting the projectile and target. If -3m/s $\leq v_x \leq$ 3m/s, then set Δv_n to 0.

(6) If the seeker head detects $-9° \leq \beta = \lambda - psi \leq 0°$, further calculate the component of the interceptor's relative speed to the target along the normal to the line connecting the projectile and target. If $v_x \geq$ 3m/s, then set the computed value of Δv_n to be negative and round it down.

(7) If the seeker head detects $-9° \leq \beta = \lambda - psi \leq 0°$, further calculate the component of the interceptor's relative speed to the target along the normal to the line connecting the projectile and target. If $v_x \leq$ -3m/s, then round up the calculated value of Δv_n.

(8) If the seeker head detects $-9° \leq \beta = \lambda - psi \leq 0°$ further calculate the component of the interceptor's relative speed to the target along the normal to the line connecting the projectile and target. If -3m/s $\leq v_x \leq$ 3m/s, then set Δv_n to 0.

(9) If the distance between the interceptor and the target is R≤10m, then stop the calculation.

6. Guidance law simulation

6.1. Guidance law simulation design

To verify the feasibility of the above-mentioned guidance law, mathematical simulations are conducted. The simulation parameters and errors are shown in **Table 1**.

Table 1. Guidance law feasibility simulation parameters

Simulation parameters	Value
Total time (s)	80
Step size (s)	0.1
Guidance gain	3
Initial relative position (m)	15,000
Initial relative velocity (m/s)	200
Interceptor precession angle (deg)	(0,1)
Interceptor nutation angle (deg)	(0,1.2)
Interceptor X-coordinate error (m)	(0,100)
Interceptor Y-coordinate error (m)	(0,100)
Interceptor impulse error	(0,5%)
Seeker angle measurement accuracy error (deg)	(0,0.1)
Pulse engine impulse error (m/s)	(0,0.1)
Single pulse engine velocity increment (m/s)	1

The single simulation lasted 74.8 s, with an error of 7.5678 m, as shown in **Figure 5**.

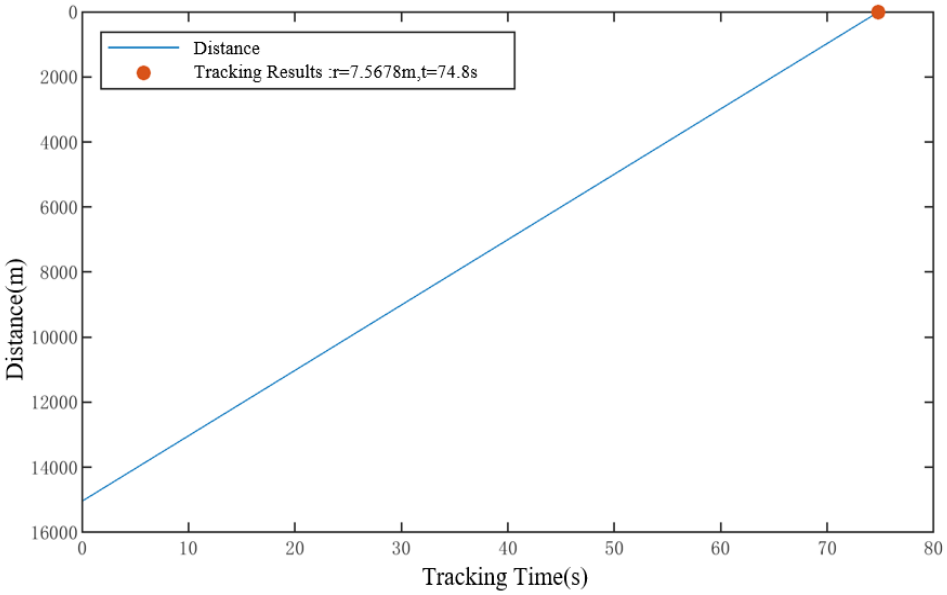

Figure 5. Tracking distance as a function of tracking time graph

From **Figure 5**, it can be seen that initially, the interceptor was 15,000 m (15 km) away from the target. After 74.8 s of guided pursuit, the final distance between the interceptor and the target was 7.5678 m. The change in distance follows a linear function, indicating that the interceptor consistently approached the target at a constant speed, with virtually no change in the velocity direction of the interceptor relative to the line connecting to the target.

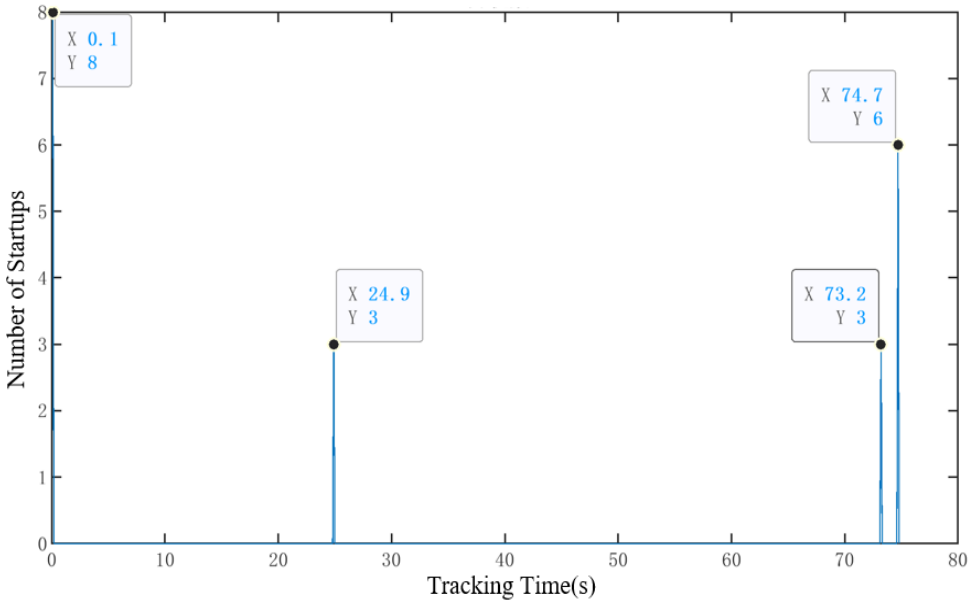

Figure 6. Number and timing distribution of pulse engine startups

From **Figure 6**, it is seen that the entire guidance process involved four startup corrections, using a total of 20 pulse engines. At 0.1 s, 8 pulse engines were started, providing a lateral velocity increment of 8 m/s, indicating an initial coordinate error in the interceptor. At 24.9 s, 3 engines were started, providing a lateral velocity increment of 3 m/s. At 74.7 s, 6 engines were started, providing a lateral velocity increment of 6 m/s. The four startups were non-continuous with significant intervals, indicating that the startup thresholds were appropriately set.

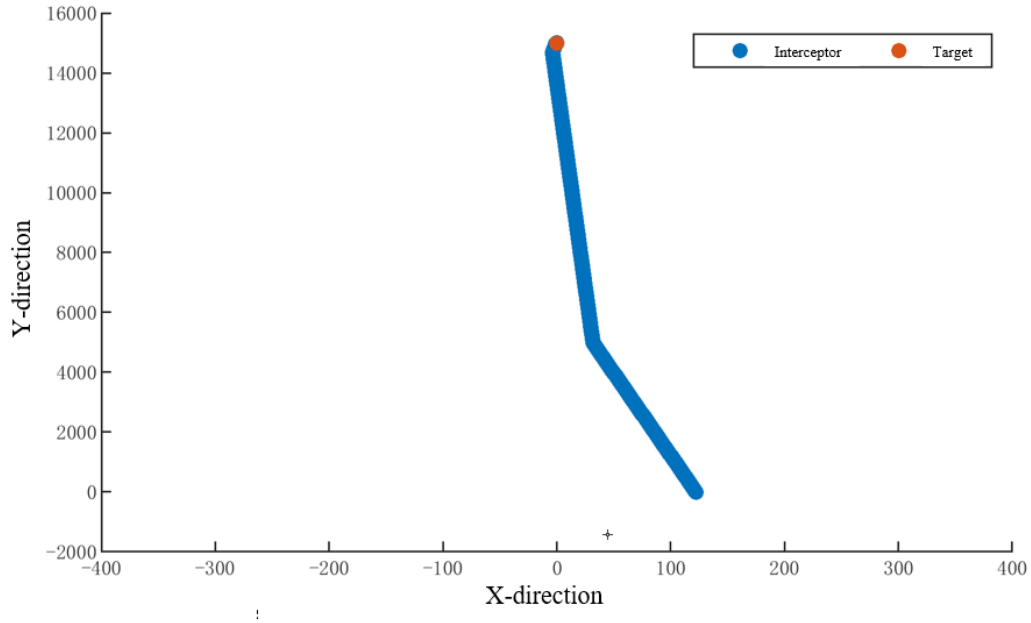

Figure 7. Interceptor coordinate change graph

From **Figure 7**, an initial error in the x-coordinate and an initial distance of 15,000 m in the y-direction to the target are observed. The distances in both the x and y directions decrease uniformly in segments, mainly closing in on the target in the y-direction. There is a turning point in the approach process where the rate of distance change in the x-direction increases significantly, indicating a major change in the interceptor's velocity direction and corrective action by pulse engine startups.

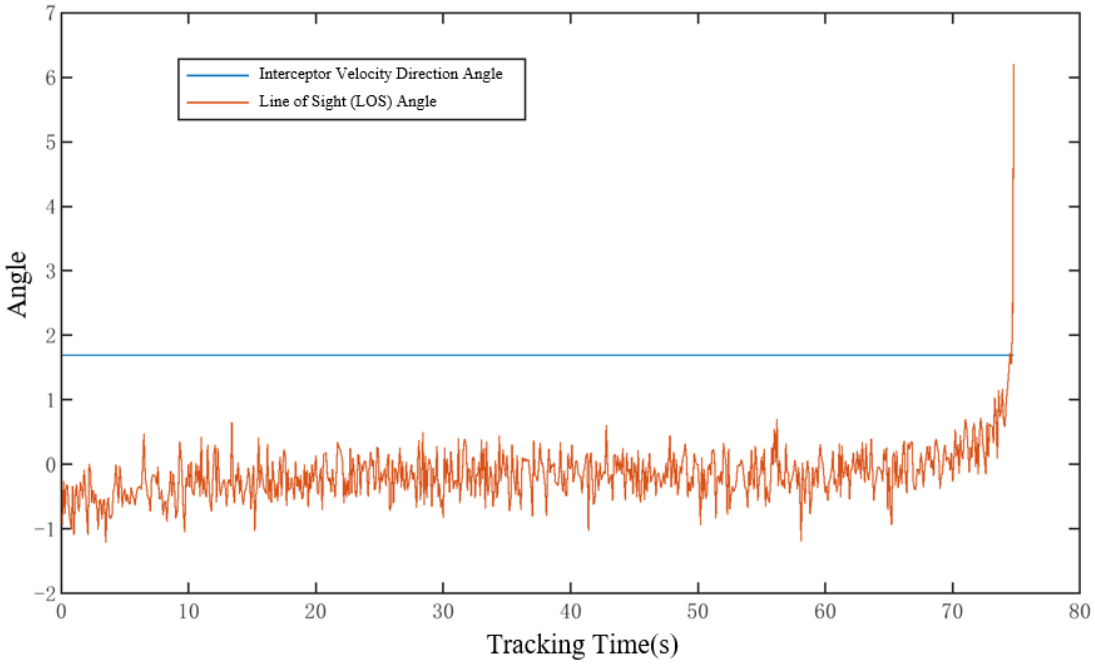

Figure 8. Changes in interceptor velocity direction angle and projectile line of sight angle over tracking time

From **Figure 8**, it can be observed that the interceptor's velocity direction angle remains constant at 1.8°, while the projectile line of sight angle exhibits an oscillating curve. The initial value measured by the seeker head was -0.5°, which gradually increases during the continuous flight until a sudden increase when closest to the

target, indicating that the guidance rate effectively suppresses the difference between the interceptor's velocity direction angle and the projectile line of sight angle, allowing the interceptor to approach the target within a certain precision range.

Monte Carlo simulation is a numerical computation technique based on random sampling methods, which handles highly uncertain statistical problems by generating a large number of random samples that follow a specific distribution.

To determine the feasibility of the guidance law, 3,000 Monte Carlo simulations were conducted, with a minimum error of 0.0448 m, a maximum error of 433.8011 m, an average error of 11.2994 m, and a mean square error of 18.1177. The error distribution from these 3,000 simulations is shown in **Figure 9**.

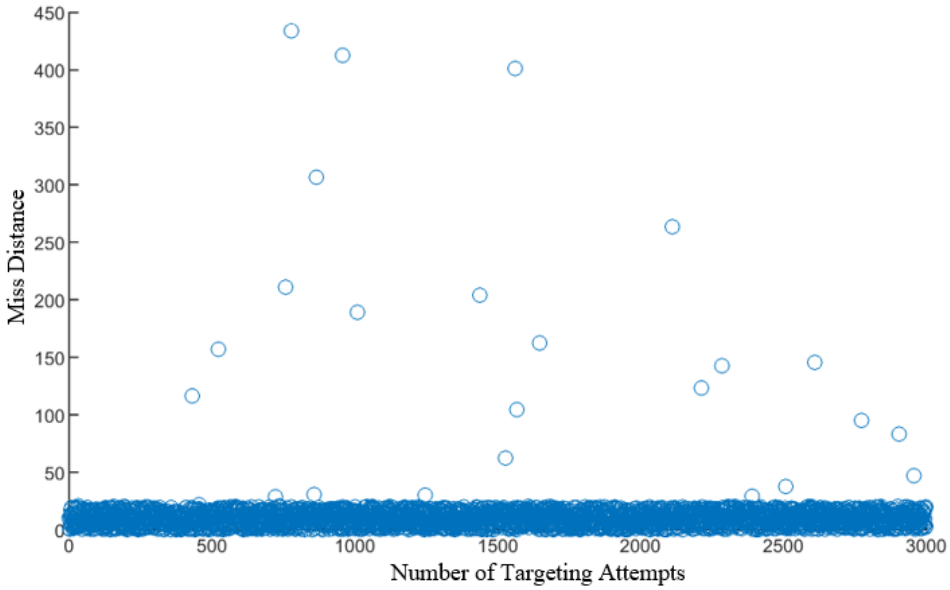

Figure 9. Range of error distribution from 3,000 simulations

In the above figure, 99.98% of errors are less than 25 m, meeting the precision requirements designed for the guidance law.

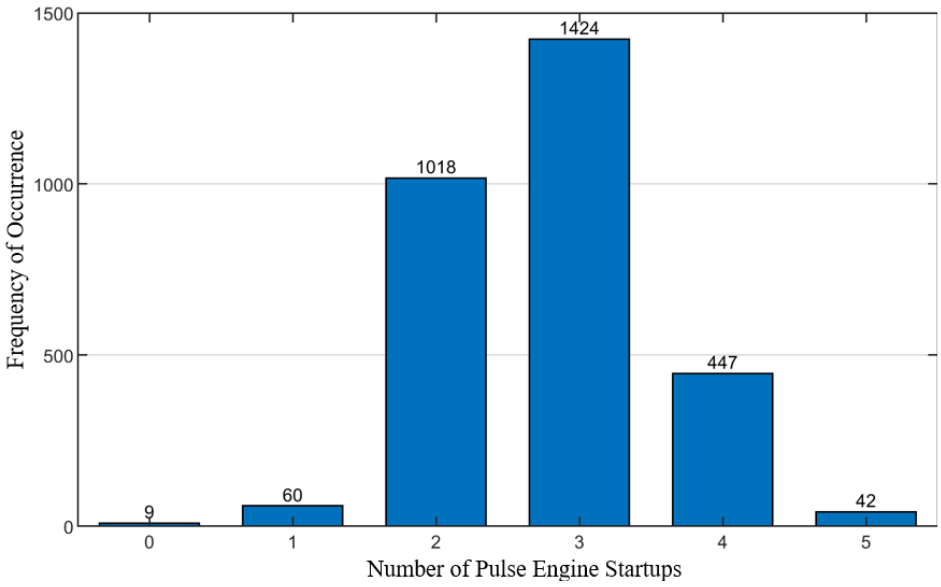

Figure 10. Pulse engine correction frequency graph

From **Figure 10**, the number of pulse engine startup corrections for velocity direction ranges from 0 to 5 times. The frequency histogram of correction counts approximately follows a normal distribution, with an average of 2.7887 corrections per 3,000 simulations, and the probability of having no more than 4 corrections is 98.6%. The frequency of engine usage is shown in **Figure 11**.

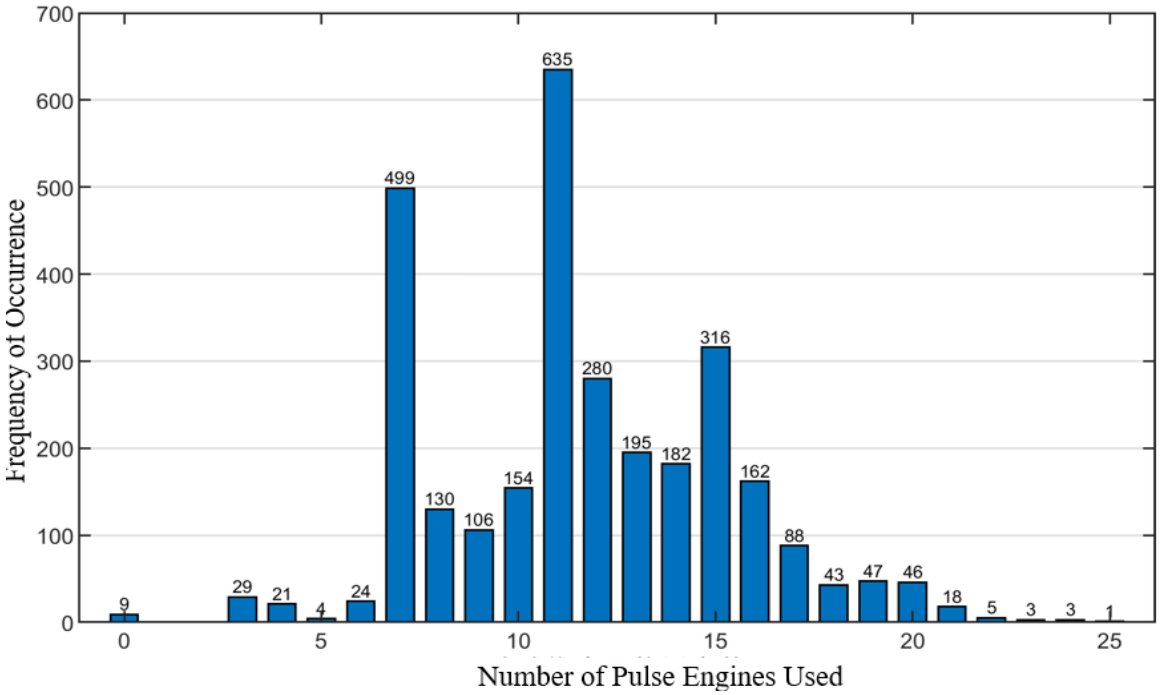

Figure 11. Statistical chart of engine usage frequency

From the figure, in 3,000 Monte Carlo simulations, the maximum number of engines used is 25, and the minimum is 0, with velocity increments ranging from 0 m/s to 25 m/s, and an average of 11.6197 engines used. Among these simulations, using 11 engines occurred the most frequently, 635 times, accounting for 21.16%. The probability of using no more than 20 engines is 99%.

In summary, this guidance law significantly improves targeting accuracy by controlling the change in angle between the interceptor's velocity direction and the line to the target. The relatively few engine corrections prevent overload due to frequent computations by the interceptor's computer, suiting the needs of space missions.

7. Conclusion

This paper proposes a guidance law for kinetic interceptors. A relative motion model of the interceptor is established, incorporating a discretized guidance law based on an improved proportional navigation method, tailored to the characteristics of the pulse engine. The thrust characteristics of the pulse engine are considered, and the corresponding startup logic is defined. The feasibility of the guidance law is verified through simulation.

Funding

(1) The National Natural Science Foundation of China (Project No. 52102436)

(2) The Natural Science Foundation of Shanghai (Project No. 23ZR1462700)

(3) The National Key Laboratory Open Fund for Strength and Structural Integrity (Project No.

ASSIKFJJ202304006)
(4) The Shanghai Aerospace Science and Technology Innovation Fund (Project No. SAST2022-031)
(5) The National Key Laboratory of Space Intelligent Control (Project No. 2023-JCJQ-LB-006-14)
(6) The Shanghai Key Laboratory of Spacecraft Mechanism (Project No. YY-F805202210025)

Disclosure statement

The authors declare no conflict of interest.

References

[1] Zhan X, Han P, Chen P, 2013, Design of Terminal Guidance Law for Kinetic Interceptors based on Nonlinear Terminal Sliding Mode. Journal of Northwestern Polytechnical University, 31(2): 233–238.

[2] Erer KS, Merttopcuoglu O, 2012, Indirect Impact-Angle-Control Against Stationary Targets using Biased Pure Proportional Navigation. Journal of Guidance, Control, and Dynamics, 35(2): 700–703. https://doi.org/10.2514/1.52105

[3] Lee CH, Kim Th, Tahk Mj, 2013, Interception Angle Control Guidance using Proportional Navigation with Error Feedback. Journal of Guidance, Control, and Dynamics, 36(5): 1556–1561.

[4] Lu P, Doman DB, Schierman JD, 2006, Adaptive Terminal Guidance for Hypervelocity Impact in Specified Direction. Journal of Guidance, Control, and Dynamics, 29(2): 269–278.

[5] Ratnoo A, Ghose D, 2008, Impact Angle Constrained Interception of Stationary Targets. Journal of Guidance, Control, and Dynamics, 31(6): 1816–1821.

[6] Tian H, Liang X, Jia X, 2011, Target Observability Criteria from Bearing-Rate-Only measurements. Journal of Beijing University of Aeronautics and Astronautics, 37(5): 534–537.

[7] Tian H, Liang X, Jia X, 2012, Research of Effect of Line-of-Sight Rate Measurement Disturb on Navigation System. Journal of Ballistics, 24(3): 65–69.

[8] Zhang Ya, Ma Gx, Lu Al, 2013, Guidance Law with Impact Time and Impact Angle Constraints. Chinese Journal of Aeronautics, 26(4): 960–966.

[9] Huang J, Zhang Y, Liu Y, 2016, A Biased Proportional Guidance Algorithm for Moving Target with Impact Angle and Field-of-View Constraints. Journal of Astronautics, 37(2): 195–202.

[10] Gu J, Chen W, 2013, Homing Guidance with Look Angle and Impact Angle Constraints. Journal of Astronautics, 34(6): 782–787.

[11] Yan L, Zhao J, Li Y, 2015, Guidance Law with Angular Constraints for Head-Pursuit or Head-on Engagement. Journal of Beijing University of Aeronautics and Astronautics, 41(5): 857–862.

[12] Li Y, Zhao J, Yan L, et al., 2015, Biased Proportional Navigation Guidance Law for Maneuvering Targets Interception with Angular Constraints. Journal of Equipment Academy, 26(5): 71–76.

[13] Turgut ET, Rosen MA, 2012, Relationship between Fuel Consumption and Altitude for Commercial Aircraft during Descent: Preliminary Assessment with a Genetic Algorithm. Aerospace Science and Technology, 17(1): 65–73.

[14] Baklacioglu T, 2016, Modeling the Fuel Flow Rate of Transport Aircraft during Flight Phases using Genetic Algorithm-Optimized Neural Networks. Aerospace Science and Technology, 49: 526–536.

[15] Zhang HF, Wang XH, Chen XF, 2015, Support Vector with ROC Optimization Method based Fuel Consumption Modeling for Civil Aircraft. Procedia Engineering, 99: 296–303.

[16] Zheng LW, Jing WX, Gu LX, 2007, A Terminal Guidance Law For Exoatmospheric Kill Vehicle. Acta Aeronautica et Astronautica Sinica, 28(4): 953–958.

[17] Zhu B, Quan Q, Cai KY, 2007, BP Networks Method of Handover Point of KKV. Journal of Beijing University of Aeronautics and Astronautics, 33(3): 332–335.